

Breakdown of the Born-Oppenheimer approximation in LiH and LiD

Ville J. Härkönen*

Computational Physics Laboratory, Tampere University, P.O. Box 692, FI-33014 Tampere, Finland

(Dated: April 5, 2024)

We compute the ab-initio electron density beyond the Born-Oppenheimer approximation in crystalline LiH and LiD with density functional methods. We report significant beyond Born-Oppenheimer corrections to electron density in the vicinity of nuclei equilibrium positions. We thus verify the breakdown of the Born-Oppenheimer approximation, as earlier suggested on experimental grounds. A reasonable agreement between the experimental and computational results is found. The results indicate the existence of beyond Born-Oppenheimer effects in solids at normal pressures and suggest that these effects can be significant also in solids containing elements other than hydrogen as well.

I. INTRODUCTION

The cornerstone of our current understanding of molecules and solids is the Born-Oppenheimer (BO) approximation [1, 2], which makes the full quantum mechanical electron-nuclear many-body problem computationally more feasible. It relies on the mass difference between nuclei and electrons and has proven to hold for a great majority of molecules and solids. One well-known exception is the LiH molecule, where the BO breakdown is well documented, and the molecule has been studied by experimental [3] and computational [4–6] methods.

The crystalline LiH, among other lithium hydrides, is of scientific interest due to the high-temperature superconductivity recently discovered in hydrides [7–10] and due to their potential as hydrogen storage [11, 12]. The X-ray diffraction experiments conducted around 30 years ago, measuring electron density, suggest the breakdown of the Born-Oppenheimer approximation in crystalline LiH [13]. There have also been subsequent theoretical, computational and experimental studies suggesting the breakdown of the BO approximation in various hydrides [14–16]. However, while ab-initio computations of electronic [17–19] and lattice dynamical properties [20] of LiH have been established, there are no computational studies which would have taken the beyond-BO effects into account in crystalline LiH.

Here we establish the first beyond-BO computation of electron density in crystalline LiH with density functional methods and computationally verify the breakdown of the BO approximation suggested by experiments [13]. Our approach is based on the results recently derived from the beyond-BO Green's function theory [21, 22] and the exact factorization of this theory [23]. We summarize the theoretical background in Sec. II and give the calculational details in Sec. III. The computed beyond-BO electron densities are represented in Sec. IV A and we make a comparison with the experimental results in Sec. IV B.

II. THEORY

The starting point of the approach used here is the many-body Coulomb problem of electrons and nuclei described by the Coulomb Hamiltonian H . The solution of the Schrödinger equation $H\Psi(\mathbf{r}, \mathbf{r}) = E\Psi(\mathbf{r}, \mathbf{r})$ is not computationally feasible, in general. In the seminal work by Born and Oppenheimer [1], it was shown that the exact problem can be separated into two parts: one for the electrons and one for the nuclei [2]

$$H_n\chi(\mathbf{R}) = E\chi(\mathbf{R}), \quad (1)$$

$$H_{BO}\Phi_{\mathbf{R}}(\mathbf{r}) = \epsilon_{BO}(\mathbf{R})\Phi_{\mathbf{R}}(\mathbf{r}), \quad (2)$$

where the nuclear (H_n) and electronic BO Hamiltonians (H_{BO}) are of the form

$$H_{BO} = H - T_n, \quad H_n = T_n + \epsilon_{BO}. \quad (3)$$

Here, T_n is the nuclear kinetic energy and ϵ_{BO} the BO energy from Eq. 2. In some systems the BO approximation, Eqs. 1 and 2 as separate entities, fails. For these kinds of situations alternative approaches have been developed [24–30] since the beyond-BO wave function approach is not computationally feasible in numerous cases, including solids. One of these alternative approaches is the beyond-BO many-body Green's function theory [21, 31], which allows the computation of exact observables like electron density. However, the general form is not computationally feasible and to overcome this limitation we combined the exact factorization [25–27, 32–35] and Green's function approaches [23]. The exact factorization of the Green's function theory [23] provides a systematic way for deriving approximations beyond-BO. In particular, it was shown that the lowest order beyond-BO approximation to electron density can be written as [23]

$$n(\mathbf{r}) = \int d\mathbf{R} |\chi(\mathbf{R})|^2 n_{\mathbf{R}}(\mathbf{r}). \quad (4)$$

Here, $n_{\mathbf{R}}(\mathbf{r})$ is the BO electron density extractable from Eq. 2 and $\chi(\mathbf{R})$ the nuclear wave function satisfying Eq. 1. The electron density $n_{\mathbf{R}}(\mathbf{r})$ can be computed by using computational packages like Quantum Espresso [36].

* ville.j.harkonen@gmail.com

We can solve the BO nuclear equation in the harmonic approximation, which holds for a wide range of materials, given no significant anharmonicity appears. The integral in Eq. 4 is demanding to compute since we have to solve $n_{\mathbf{R}}(\mathbf{r})$ for all nuclear configurations that the integral goes through. If we assume the harmonic approximation to solve the BO nuclear equation for the m th harmonic eigenstate, $\chi(\mathbf{R}) = \chi_m(\mathbf{R})$, it is beneficial to approximate Eq. 4 as follows. We carry out the conventional coordinate transformation of lattice dynamics [2] $\mathbf{R} = \mathbf{x} + \mathbf{u}$, where \mathbf{x} are parameters called the reference positions and \mathbf{u} are the displacements (quantum mechanical variables) from the reference positions. We expand $n_{\mathbf{R}}(\mathbf{r}) = n_{\mathbf{x}+\mathbf{u}}(\mathbf{r})$ up to third order in \mathbf{u} about \mathbf{x} and Eq. 4 can be written as

$$n_m(\mathbf{r}) \approx n_{\mathbf{x}}(\mathbf{r}) + \frac{1}{2} \sum_{s_1, s_2} \frac{\partial^2 n_{\mathbf{x}}(\mathbf{r})}{\partial x_{s_1} \partial x_{s_2}} \langle m | \hat{u}_{s_1} \hat{u}_{s_2} | m \rangle. \quad (5)$$

Here we used the fact that the first and third order terms vanish since we assumed the harmonic eigenstates. In Eq. 5, $s_i = \alpha_i k_i$ is the combined label for Cartesian index α_i and the label for the k_i th nucleus. We can incorporate temperature dependence by taking harmonic canonical thermal average of Eq. 5 with respect to the nuclear states, namely

$$\langle n(\mathbf{r}) \rangle = n_{\mathbf{x}}(\mathbf{r}) + \frac{1}{2} \sum_{s_1, s_2} \frac{\partial^2 n_{\mathbf{x}}(\mathbf{r})}{\partial x_{s_1} \partial x_{s_2}} \langle \hat{u}_{s_1} \hat{u}_{s_2} \rangle. \quad (6)$$

We denote the last term of Eq. 6 as $\langle n'_{\mathbf{x}}(\mathbf{r}) \rangle \equiv \frac{1}{2} \sum_{s_1, s_2} \frac{\partial^2 n_{\mathbf{x}}(\mathbf{r})}{\partial x_{s_1} \partial x_{s_2}} \langle \hat{u}_{s_1} \hat{u}_{s_2} \rangle$ and use the following notation for the ensemble average

$$\langle \hat{o} \rangle = \sum_m p_m \langle m | \hat{o} | m \rangle, \quad p_m = \frac{e^{-\beta E_m}}{\sum_{m'} e^{-\beta E_{m'}}}, \quad (7)$$

where E_m is the eigenvalue of the m th eigenstate of the harmonic nuclear Hamiltonian. The quantities needed to compute $\langle n(\mathbf{r}) \rangle$ are therefore the equilibrium BO electron density $n_{\mathbf{x}}(\mathbf{r})$, its second order mixed partial derivatives and the covariance $\langle \hat{u}_{s_1} \hat{u}_{s_2} \rangle$ [37, 38]. We compute these quantities by using open source ab-initio computational package Quantum Espresso (QE) [36], which is based on density functional theory [39, 40]. The QE program package has been successfully used to predict various experimentally relevant quantities of interest [41] within BO approximation, including phonon related properties [42–44].

III. CALCULATIONAL DETAILS

With QE (version 7.0), we use projector augmented-wave method [45] and PBE functional [46]. The harmonic phonon frequencies are computed by using the density functional perturbation theory as implemented in QE [47]. The plane wave kinetic energy and charge

density cut-off values used were 80 Ry and 560 Ry, respectively. The electronic structure was computed with $20 \times 20 \times 20$ \mathbf{k} point grids. We constructed $2 \times 2 \times 2$ supercells in order to compute the electron density derivatives of Eq. (6). The derivatives were computed as finite central differences with 0.5% displacements from the nuclear equilibrium positions. To compute the electron density corrections from Eq. (6) we computed the lattice dynamical properties with the \mathbf{q} point meshes matching the supercell dimensions. The structure parameters for LiH ($Fm\bar{3}m$), which define the structure, are given in Table 1 of [13]. The LiH structure parameters used are the following: lattice parameter $a = 4.0609$ Å; fractional coordinates of the inequivalent atoms Li= (0.000, 0.000, 0.000), H= (0.500, 0.000, 0.000). We first established the structure relaxation of the structure with the given parameters after which the lattice dynamical properties were computed. The equilibrium structure of LiD is identical to LiH in the BO approximation. All the calculations are established at 0 kbar pressure.

IV. RESULTS

A. Beyond Born-Oppenheimer electron density

The conventional unit cell of the LiH crystal structure is given in Fig. 1(a) and the phonon dispersions for LiH and LiD in Fig. 1(b). The phonon dispersion closely resembles to that obtained in earlier studies [20, 48]. The acoustic modes of LiH and LiD are rather close to identical implying that these modes almost completely consist of vibrations of Li atoms. As expected, the optical modes in LiD are scaled down relative to the corresponding modes of LiH due to the higher mass of deuterium.

The relative change $[\langle n(\mathbf{r}) \rangle - n_{\mathbf{x}}(\mathbf{r})] / n_{\mathbf{x}}(\mathbf{r}) = \langle n'_{\mathbf{x}}(\mathbf{r}) \rangle / n_{\mathbf{x}}(\mathbf{r})$ in electron density in the 100-plane of the conventional cell [see Fig. 1(a)] is depicted in Fig. 1(c). Moreover, electron densities along different lines of the 100-plane are given by Figs. 1(d)-1(f). We see a significant breakdown of the BO approximation. The largest relative change is around -76%/-82% (0 K/300 K) at the hydrogen nuclear equilibrium positions and around -47%/-75% (0 K/300 K) at the lithium equilibrium positions. The largest positive relative change is in the surrounding volumes of the Li nuclear positions. The relative change is positive in the large volumes between the nuclei. In the case of LiD, the largest relative change is around -53%/-62% (0 K/300 K) at the deuterium nuclear equilibrium positions, the changes around Li nuclei being essentially identical to that in LiH. The breakdown is more significant at higher temperatures, especially in the vicinity of the heavier nuclei, lithium and deuterium. We see drastic deviations at 300 K as the BO values are about five times higher than the beyond-BO values at the equilibrium positions of hydrogen and lithium. The functional form of the beyond-BO and BO densities at 0 K is the same around the Li nuclei, but around the

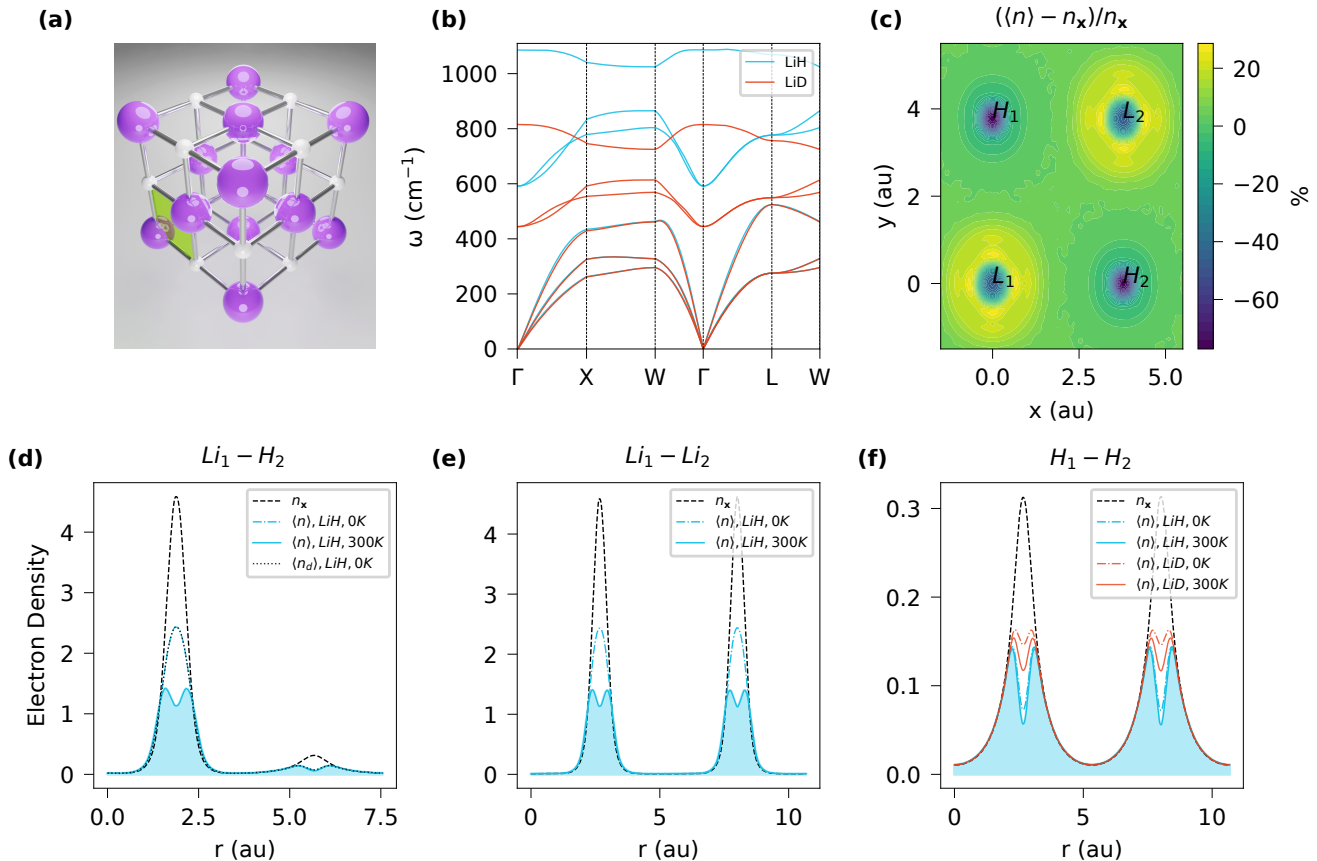


FIG. 1. Phonon dispersions for LiH and LiD and electron densities (pseudo) in 100-plane of the conventional unit cell (110-plane of the primitive cell) and in selected lines along the 100-plane. The electron densities are normalized to the number of (valence) electrons per unit cell. (a) The conventional unit cell with the 100-plane indicated with a green plane in the lower left corner (b) phonon dispersions for LiH and LiD (c) the difference of beyond-BO and BO densities relative to $n_x(\mathbf{r})$ in percentage at 0 K, (d) electron densities along the line between lithium nuclei (pointed out in c), (e) between lithium and hydrogen and (f) between hydrogen nuclei. In (d), $\langle n_d \rangle$ denotes the diagonal contribution to $\langle n \rangle$ discussed in the text. We have left out the lines for LiD in (d) and (e) since in the vicinity of lithium nuclei the results are essentially identical.

hydrogen(deuterium) nuclei, the change from unimodal to bimodal functional shape occurs. At 300 K the functional forms of the densities near all nuclei, including lithium, change from unimodal to bimodal shape. In Fig. 1(d), the diagonal elements of Eq. 6 are depicted and these terms essentially explain the whole beyond-BO effect. The change in electron density at a given point in space is thus caused by a local position uncertainty of the nucleus, which is the same mechanism that occurs in the YH_6 superconductor and Cs-IV phase of solid hydrogen [38].

B. Comparison with experiment

Our findings support the suggested breakdown of the BO approximation based on experiments [13, 49]. We verify the difference in densities of LiH and LiD in the volumes near H and D nuclei, which is a sign of BO break-

down and was noted in [13]. The measurements cannot be made within the BO approximation and thus are not, at least directly, able to distinct the breakdown near the Li nuclei. Our results show a significant reduction of electron density at the volumes near the nuclear equilibrium positions of all three species of elements. The results also indicate that the breakdown occurs in both studied states of matter.

The computed spherically averaged radial densities with the previous experimental results at 293 K [13] for LiH are depicted in Fig. 2. Both, the pseudo and all-electron densities are given. At low radii range (below ~ 0.1 au), we have numerical instabilities in the computation of all-electron density derivatives. The radial BO density is flattened for both species by the beyond-BO effects. For lithium, the computed values are rather close to the experimental ones at low and high radii ranges. The largest differences are at around ~ 0.5 au radius. The beyond-BO densities, in comparison to the corre-

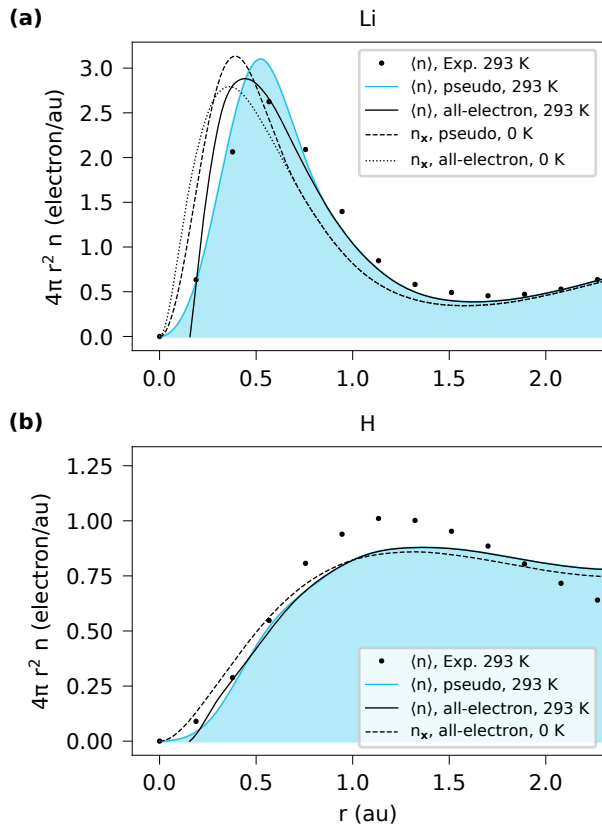


FIG. 2. Spherically averaged radial electron densities in LiH. (a) For Li nucleus (b) for H nucleus. The computed pseudo and all electron densities are given. The experimental data at 293 K is from Ref. [13]. Some numerical instabilities were detected in the all-electron density derivatives, which manifest themselves in the beyond-Born-Oppenheimer all-electron curves at small radii away from the nuclei.

sponding BO densities, are closer to the experimental values essentially in the whole range considered. In the middle radii range, the experimental density is further flattened in comparison to our computational result and the curve is peaking around ~ 0.1 au later. The results for hydrogen follow along the similar lines: the smallest deviations are obtained at lowest radii and the largest deviation appears in the middle range. In this case the experimental results imply higher values at the middle range, which is the opposite to what we found for lithium. Again, the BO densities are the furthest away from the experimental values essentially the whole range considered. There are several factors that can cause these mentioned differences. Possible factors are errors originating from the density functional used and the neglected of anharmonicity. We note, however, that the computed phonon dispersions here are consistent with earlier computational results, which appear to closely match the experimental findings. [48]. This implies a relatively weak

anharmonicity. It remains to be seen if the computational result about the bimodal shapes of the density at the nuclei equilibrium positions, visible in Fig. 1, can be verified by modern experimental methods [50, 51]. It appears that the current experimental data with the model used [13] to refine the experimental X-ray data does not repeat these features.

V. CONCLUSION

We have studied beyond-BO corrections to the electronic structure of LiH and LiD and report a significant failure of the BO approximation, particularly apparent in volumes near the nuclei. The temperature dependence of electron density was found to be stronger at the vicinity of the heavier nuclei. While the our computational results compare rather well to the earlier experimental results there still remains room for improvement, like the inclusion of anharmonicity.

Earlier computational results on YH_6 superconductor and Cs-IV phase of hydrogen [38] imply the failure of BO approximation in phases of matter that exist at high pressures. Here we show that the BO approximation can also fail in states of matter that exist at low pressures and that the mechanism of the breakdown is local position uncertainty of the nuclei. Another important aspect indicated by the results is that a significant BO breakdown can occur in elements other than hydrogen, lithium and deuterium in the present case. The lithium is around seven times more massive than hydrogen which suggests that there could be relevant beyond-BO effects in a number of different solids. For instance, carbon has less than twice the mass of lithium.

To summarize. We report a significant breakdown of the BO approximation in LiH and LiD, which is verified by computing the ab-initio beyond-BO electron density with density functional methods. The results support the earlier experimental findings and recent computational findings in solid hydrogen and in YH_6 superconductor [38]. Our recent findings highlight the importance of beyond-BO effects in solids, which are likely necessary to consider in order to enhance our understanding of materials such as various hydrides and solid hydrogen.

ACKNOWLEDGMENTS

The author acknowledges Prof. E. K. U. Gross for numerous discussions on beyond-BO physics over the years. The author gratefully acknowledges funding from the Magnus Ehrnrooth foundation and Jenny and Antti Wihuri foundation. The computing resources for this work were provided by CSC - the Finnish IT Center for Science.

-
- [1] M. Born and R. Oppenheimer, *Ann. Phys. (Leipzig)* **389**, 457 (1927).
- [2] K. Huang and M. Born, *Dynamical Theory of Crystal Lattices* (Clarendon Press Oxford, 1954).
- [3] L. Wharton, L. P. Gold, and W. Klemperer, *J. Chem. Phys.* **37**, 2149 (1962).
- [4] M. Cafiero, S. Bubin, and L. Adamowicz, *Phys. Chem. Chem. Phys.* **5**, 1491 (2003).
- [5] S. Bubin, L. Adamowicz, and M. Molski, *J. Chem. Phys.* **123** (2005).
- [6] S. Bubin, M. Cafiero, and L. Adamowicz, *Adv. Chem. Phys.* **131**, 377 (2005).
- [7] Y. Xie, Q. Li, A. R. Oganov, and H. Wang, *Acta Crystallog. Sect. C* **70**, 104 (2014).
- [8] A. Drozdov, M. Erements, I. Troyan, V. Ksenofontov, and S. I. Shylin, *Nature* **525**, 73 (2015).
- [9] A. Drozdov, P. Kong, V. Minkov, S. Besedin, M. Kuzovnikov, S. Mozaffari, L. Balicas, F. Balakirev, D. Graf, V. Prakapenka, *et al.*, *Nature* **569**, 528 (2019).
- [10] M. Somayazulu, M. Ahart, A. K. Mishra, Z. M. Geballe, M. Baldini, Y. Meng, V. V. Struzhkin, and R. J. Hemley, *Phys. Rev. Lett.* **122**, 027001 (2019).
- [11] T. Ichikawa, N. Hanada, S. Isobe, H. Leng, and H. Fujii, *J. Phys. Chem. B* **108**, 7887 (2004).
- [12] N. Klopčič, I. Grimmer, F. Winkler, M. Sartory, and A. Trattner, *J. Energy Storage* **72**, 108456 (2023).
- [13] R. Vidal-Valat, J.-P. Vidal, K. Kurki-Suonio, and R. Kurki-Suonio, *Acta Crystallog. Sect. A* **48**, 46 (1992).
- [14] N. I. Gidopoulos, *Phys. Rev. B* **71**, 054106 (2005).
- [15] M. Krzystyniak and F. Fernandez-Alonso, *Phys. Rev. B* **83**, 134305 (2011).
- [16] M. Krzystyniak, S. E. Richards, A. G. Seel, and F. Fernandez-Alonso, *Phys. Rev. B* **88**, 184304 (2013).
- [17] S. Baroni, G. Pastori Parravicini, and G. Pezzica, *Phys. Rev. B* **32**, 4077 (1985).
- [18] M. J. van Setten, V. A. Popa, G. A. de Wijs, and G. Brocks, *Phys. Rev. B* **75**, 035204 (2007).
- [19] A. Reshak, *Int. J. Hydrogen Energy* **38**, 11946 (2013).
- [20] S. Biswas, I. Errea, M. Calandra, F. Mauri, and S. Scandolo, *Phys. Rev. B* **99**, 024108 (2019).
- [21] V. J. Härkönen, R. van Leeuwen, and E. K. U. Gross, *Phys. Rev. B* **101**, 235153 (2020).
- [22] V. J. Härkönen, arXiv:2403.16103 (2024).
- [23] V. J. Härkönen, *Phys. Rev. B* **106**, 205137 (2022).
- [24] T. Kreibich and E. K. U. Gross, *Phys. Rev. Lett.* **86**, 2984 (2001).
- [25] N. I. Gidopoulos and E. K. U. Gross, arXiv:cond-mat/0502433 (2005).
- [26] N. I. Gidopoulos and E. K. U. Gross, *Phil. Trans. R. Soc. A* **372**, 20130059 (2014).
- [27] A. Abedi, N. T. Maitra, and E. K. U. Gross, *Phys. Rev. Lett.* **105**, 123002 (2010).
- [28] E. Villaseco Arribas, F. Agostini, and N. T. Maitra, *Molecules* **27**, 4002 (2022).
- [29] A. Muolo, A. Baiardi, R. Feldmann, and M. Reiher, *J. Chem. Phys.* **152**, 204103 (2020).
- [30] R. Feldmann, A. Muolo, A. Baiardi, and M. Reiher, *J. Chem. Theory Comput.* **18**, 234 (2022).
- [31] G. Baym, *Ann. Phys.* **14**, 1 (1961).
- [32] G. Hunter, *Int. J. Quant. Chem.* **9**, 237 (1975).
- [33] A. Abedi, N. T. Maitra, and E. Gross, *J. Chem. Phys.* **137**, 22A530 (2012).
- [34] A. Schild, F. Agostini, and E. Gross, *J. Phys. Chem. A* **120**, 3316 (2016).
- [35] F. Agostini and E. K. U. Gross, Exact factorization of the electron–nuclear wave function: Theory and applications, in *Quantum Chemistry and Dynamics of Excited States* (John Wiley & Sons, 2020) Chap. 17, pp. 531–562.
- [36] P. Giannozzi, S. Baroni, N. Bonini, M. Calandra, R. Car, C. Cavazzoni, D. Ceresoli, G. L. Chiarotti, M. Cococcioni, I. Dabo, *et al.*, *J. Phys.: Condens. Matter* **21**, 395502 (2009).
- [37] V. J. Härkönen and A. J. Karttunen, *Phys. Rev. B* **89**, 024305 (2014).
- [38] V. J. Härkönen, arXiv:2311.06114 (2023).
- [39] P. Hohenberg and W. Kohn, *Phys. Rev.* **136**, B864 (1964).
- [40] W. Kohn and L. J. Sham, *Phys. Rev.* **140**, A1133 (1965).
- [41] P. Giannozzi, O. Andreussi, T. Brumme, O. Bunau, M. B. Nardelli, M. Calandra, R. Car, C. Cavazzoni, D. Ceresoli, M. Cococcioni, *et al.*, *J. Phys.: Condens. matter* **29**, 465901 (2017).
- [42] V. J. Härkönen and A. J. Karttunen, *Phys. Rev. B* **93**, 024307 (2016).
- [43] V. J. Härkönen and A. J. Karttunen, *Phys. Rev. B* **94**, 054310 (2016).
- [44] T. Tadano and W. A. Saidi, *Phys. Rev. Lett.* **129**, 185901 (2022).
- [45] P. E. Blöchl, *Phys. Rev. B* **50**, 17953 (1994).
- [46] J. P. Perdew, K. Burke, and M. Ernzerhof, *Phys. Rev. Lett.* **77**, 3865 (1996).
- [47] S. Baroni, S. de Gironcoli, A. Dal Corso, and P. Giannozzi, *Rev. Mod. Phys.* **73**, 515 (2001).
- [48] J. Zhang, L. Zhang, T. Cui, Y. Li, Z. He, Y. Ma, and G. Zou, *Phys. Rev. B* **75**, 104115 (2007).
- [49] S. Yamamura, S. Kasahara, M. Takata, Y. Sugawara, and M. Sakata, *J. Phys. Chem. Solids* **60**, 1721 (1999).
- [50] A. Genoni, L. Bučinský, N. Claiser, J. Contreras-García, B. Dittrich, P. M. Dominiak, E. Espinosa, C. Gatti, P. Giannozzi, J.-M. Gillet, *et al.*, *Chem. Eur. J.* **24**, 10881 (2018).
- [51] C. Addiego, W. Gao, H. Huyan, and X. Pan, *Nat. Rev. Phys.* **5**, 117 (2023).